

## ARTICLE

# Effect of Cellular Senescence on the Growth of HER2-Positive Breast Cancers

Mariano F. Zacarias-Fluck, Beatriz Morancho, Rocio Vicario, Antonio Luque Garcia, Marta Escorihuela, Josep Villanueva, Isabel T. Rubio, Joaquín Arribas

**Affiliations of authors:** Preclinical Research (MZF, BM, RV, ALG, ME, JV, JA) and Clinical Research Programs (ITR), Vall d'Hebron Institute of Oncology, Barcelona, Spain; Department of Biochemistry and Molecular Biology, Universitat Autònoma de Barcelona, Campus de la UAB, Bellaterra, Spain (JA); Institutió Catalana de Recerca i Estudis Avançats, Barcelona, Spain (JA).

**Correspondence to:** Joaquín Arribas, PhD, Psg. Vall d'Hebron 119-129, Barcelona 08035, Spain (e-mail: [jarribas@vhio.net](mailto:jarribas@vhio.net)).

## Abstract

**Background:** Oncogene-induced senescence (OIS) is a tumor suppressor mechanism. However, senescent cells remain viable and display a distinct secretome (also known as senescence-associated secretory phenotype [SASP] or senescence messaging secretome, [SMS]) that, paradoxically, includes protumorigenic factors. OIS can be triggered by ectopic overexpression of HER2, a receptor tyrosine kinase and the driving oncogene in a subtype of human breast cancer. However, cellular senescence has not been characterized in HER2-positive tumors.

**Methods:** Using an approach based on their inability to proliferate, we isolated naturally occurring senescent cells from a variety of tumor models including HER2-positive cells, transgenic mice ( $n = 3$ ), and patient-derived xenografts (PDXs) ( $n = 6$  mice per group from one PDX derived from one patient). Using different biochemical and cell biological techniques, we characterized the secretome of these senescent cells. All statistical tests were two-sided.

**Results:** We found that senescent cells arise constantly in different models of advanced breast cancers overexpressing HER2 and constitute approximately 5% of tumor cells. In these models, IL-6 and other cytokines were expressed mainly, if not exclusively, by the naturally occurring senescent cells (95.1% and 45.0% of HCC1954 cells and cells from a HER2-positive PDX expressing a senescent marker expressed IL-6, respectively). Furthermore, inhibition of IL-6 impaired the growth of the HER2-positive PDX (mean tumor volume at day 101, control vs anti-huIL-6 treated,  $332.2 \text{ mm}^3$  [95% confidence interval {CI} = 216.6 to 449.8] vs  $114.4 \text{ mm}^3$  [95% CI = 12.79 to 216.0],  $P = .005$ ).

**Conclusions:** Senescent cells can contribute to the growth of tumors by providing cytokines not expressed by proliferating cells, but required by these to thrive.

Senescence, a terminal cell proliferation arrest, can be triggered by an excessive number of cell divisions or a variety of stressors, including oncogenes. Oncogene-induced senescence (OIS) is considered a tumor suppressor mechanism; it impedes the expansion of early neoplastic cells before they become fully malignant (1). In contrast with premalignant cells suppressed by apoptosis, cells undergoing OIS remain metabolically active and display

a secretome completely different to that of the cell of origin. This profound change in the secretome is a hallmark of senescence and has been termed Senescence Associated Secretory Phenotype (SASP) (2), Senescence Messaging Secretome (SMS) (3), or simply senescence secretome. A distinct cellular compartment, known as TOR-autophagy spatial coupling compartment (TASCC), has been proposed as responsible for the synthesis

Received: August 12, 2014; Revised: December 4, 2014; Accepted: January 20, 2015

© The Author 2015. Published by Oxford University Press. All rights reserved. For Permissions, please e-mail: [journals.permissions@oup.com](mailto:journals.permissions@oup.com).

and secretion of components of the senescence secretome. The TASC is characterized by the localization of the Ser/Thr kinase mammalian target of rapamycin (mTOR) to autophagosomes (4).

Some components of the senescence secretome, such as the cytokines IL-6 or IL-8, are secreted by most senescent cells (2). Others seem to vary according to the cell of origin or the specific trigger that causes senescence (5,6). The secretome of some senescent cells includes components that, acting in an autocrine fashion, contribute to establishing and perpetuating the senescence program (7,8). In addition, senescence secretomes may contain chemotactic factors that attract cellular components of the innate and adaptive branches of the immune system. These recognize and eliminate senescent cells (9–12). However, not all the components of the senescence secretome seem to contribute to the antitumor effects of OIS. In fact, the presence of functional protumorigenic and prometastatic factors in the secretome of some senescent cells indicates that they may contribute to tumor progression in a cell nonautonomous manner (2). In many studies, this effect has been observed using cell-based and animal models in which OIS was triggered by the ectopic overexpression of oncogenes, such as mutated RAS or BRAF, to levels higher than those occurring in human tumors, making it difficult to extrapolate its relevance.

The receptor tyrosine kinase HER2 is a prototypic proto-oncogene that is activated through gene amplification in approximately 20% of human breast cancers (13). Intriguingly, IL-6 cooperates with HER2 during tumor progression (14,15); in fact, blocking IL-6 signaling impairs the progression of breast cancers developed by transgenic mice overexpressing HER2 (16), indicating that IL-6 secreted by senescent cells could contribute to the progression of HER2-positive breast cancers.

HER2 protein levels in tumors with HER2 gene amplification are highly variable, reaching a difference of greater than 100 fold, as estimated by continuous protein quantification analysis (17). Additionally, tumors with high levels of HER2 can also express variable levels of a carboxy-terminal fragment of HER2 known as 611CTF or p95HER2 (18–19). This fragment is an oncogenic form of HER2 because of its ability to constitutively form active homodimers maintained by intermolecular disulphide bonds (20). Thus, in HER2-positive breast cancers, the levels of HER2 signaling are highly variable.

Expression of high levels of constitutively active HER2 leads to a fully penetrant senescence phenotype characterized by a distinct secretome. This senescence secretome increases the metastatic ability of proliferating breast cancer cells (6,21). Here, we present experiments aimed to analyze the effect of lower, pathophysiologically relevant levels of HER2 signaling on the onset of senescence. We analyzed the presence of senescent cells in different models of HER2-driven tumorigenesis and characterized their role in tumor growth.

## Methods

### Confocal Microscopy

Cells were grown in coverslips, washed twice with 1X PBS, and fixed with 4% paraformaldehyde for 20 minutes. After two washes, cells were permeabilized with 0.1% Triton X-100 in 1X PBS; 1% BSA-0.1% saponin-0.02% Azide-PBS was used for blocking and antibodies binding. Finally, cells were washed and mounted with Vectashield mounting medium with DAPI (Vector Laboratories, Peterborough, UK). Cells were visualized in a confocal spectral FV 1000 Olympus microscope at 40x (Olympus Corp., Tokyo, Japan).

Fluorescence intensity corresponding to IL-6 was measured with ImageJ software as described in (22). Briefly, cells were selected using ImageJ selection tool and area and integrated density were measured. Corrected total cell fluorescence was calculated as integrated density – (area of selected cell x mean fluorescence of background readings).

### Tumor-Derived Primary Culture Establishment

Cell cultures derived from PDXs were established as described in (23). Briefly, tumors were excised and cut into the smallest pieces possible with scalpel, incubated for 30 minutes with collagenase IA, washed and resuspended in Dulbecco's Modified Eagle's Media (DMEM):F-12, 10% FBS, 4 mmol/L L-glutamine, Penicillin/Streptomycin (Gibco), 10mM HEPES (Santa Cruz), and 1.75 µg/mL Amphotericin B (Fungizone, Gibco) for six hours, then medium was carefully removed and changed to 10% supplemented Mammocult human medium (StemCell technologies) with Penicillin/Streptomycin, 10mM HEPES, and 1.75 µg/mL Amphotericin B for one week in order to facilitate the growth of epithelial cells with respect to contaminating mouse fibroblasts.

### Patient-Derived Xenografts

Six- to eight-week-old female NOD.CB17-Prkdc<sup>scid</sup>/J (NOD/SCID) were purchased from Charles River Laboratories (Paris, France). Mice were maintained and treated in accordance with institutional guidelines of Vall d'Hebron University Hospital Care and Use Committee. Fragments of patient samples were implanted into the number four fat pad of the mice (six mice per group). 17 β-estradiol (1µM) (Sigma) was added to drinking water. The breast tumor sample used in this study was from a surgical resection at Vall d'Hebron University Hospital and was obtained following the institutional guidelines. Written informed consent for the performance of tumor molecular studies was obtained from the patient who provided tissue. Histopathologic characteristics were confirmed by a pathologist and molecular characterization was carried out by analyzing the expression of 50 selected genes (23). HER2-PDX is a luminal B, HER2-positive breast tumor.

### Growth of HCC1954\_Luciferase In Vivo

HCC1954 cells were stably transfected with pLenti CMV V5-LUC Blast (w567-1) vector (24). After blasticidin selection, firefly luciferase activity was checked in vitro. 5x10<sup>5</sup> cells in 100 µL Matrigel:PBS (1:1) were injected orthotopically in the fourth fat pad of Balb/C nude mice (seven mice per group).

CNT328 (Siltuximab, 20mg/kg in sterile PBS) or antimouse IL-6 (20mg/kg in sterile PBS) were given intraperitoneally once weekly. Tumor xenografts were measured with calipers every three days, and tumor volume was determined using the formula: (length x width<sup>2</sup>) x (pi/6). At the end of the experiment, the animals were anesthetized with a 1.5% isoflurane-air mixture and were killed by cervical dislocation.

### RCAS-TVA-ErbB2 Model

RCAS vector carrying ErbB2 gene was instilled intraductally in MMTV-tva transgenic mice as described in (25,26). Briefly, a HA-tagged rat Neu cDNA insert with a Val-to-Glu point mutation of codon 664 and truncations at both extracellular and intracellular domains was cloned into an RCAS vector. DF-1 chicken

fibroblasts were transfected with RCAS vectors and maintained in 10% FBS-DMEM in humidified 5% CO<sub>2</sub> 37°C incubators. RCAS viruses present in the culture supernatant were concentrated 100-fold by centrifugation at 125 000 x g for 90 minutes, resuspended in 10% FBS-DMEM, and frozen in aliquots for titer determination and infection of animals. Finally, six-week-old female mice were anesthetized and injected through intraductal injection with high titer RCAS viruses in a 10 µL volume along with 0.1% bromophenol blue, used as a tracking dye. Tumor growth was followed by palpation. Tumors were excised at a volume of 600 mm<sup>3</sup> for further analyses and determinations.

### Proteomic Analysis

After cell sorting, cells were plated for 48 hours and then washed five times with serum-free medium and incubated for additional 48 hours in the absence of serum. The conditioned media were then collected, spun down at 1000 RPM for five minutes, transferred into clean tubes, filtered through a Nalgene 0.2mm pore vacuum filter, and concentrated using a 10 000 MWCO Millipore Amicon Ultra by spinning down 15 mL at a time at 800 g for 30 minutes until the final concentration was 1 mg/mL (~200- to 300-fold concentration). Protein concentration was determined with a Bio-Rad protein assay. Subsequent sample preparation and proteomic analysis were conducted as previously described (6). Heatmap hierarchical clustering was performed at <http://www.hiv.lanl.gov/content/sequence/HEATMAP/heatmap.html>.

### Statistical Analysis

Data are presented as averages, and error bars were analyzed by the Student's t test when comparing two groups or analysis of variance when comparing more than two groups. Results were considered to be statistically significant at a P value of less than .05. All statistical tests were two-sided. Analyses were conducted using the GraphPad Prism 5 Statistical Software.

All other methods are described in detail in the [Supplementary Methods](#) (available online).

### Results

Expression of the wild-type tyrosine kinase receptor HER2 did not affect the rate of cell proliferation (Supplementary [Figure 1A](#)); nevertheless, compared with cells transfected with the empty vector, it resulted in an increase in the percentage of cells with a flattened and vacuolated morphology, typical of senescent cells ([Figure 1A](#), arrow). HER2 expression also led to an increase in the percentage of cells positive for SA-β-gal, the most widely used marker of cellular senescence (7.3% [95% CI = 3.12% to 11.64%] in MCF7/HER2 vs 3.2% [95% CI = 0.48% to 5.94%] in MCF7/Vector,  $P = .046$ ). Furthermore, the percentage of cells positive for nuclear p21, a cyclin-dependent kinase inhibitor expressed by HER2-induced senescent cells (21), or gammaH2AX and 53BP1, two markers of the DNA damage response frequently upregulated in oncogene-induced senescent cells (reviewed in [27]), also increased with the expression of HER2 (percentage of positive cells in MCF7/HER2 vs MCF7/Vector; p21: 11.1% [95% CI = 3.123% to 11.64%] vs 2.3% [95% CI = 0.4735% to

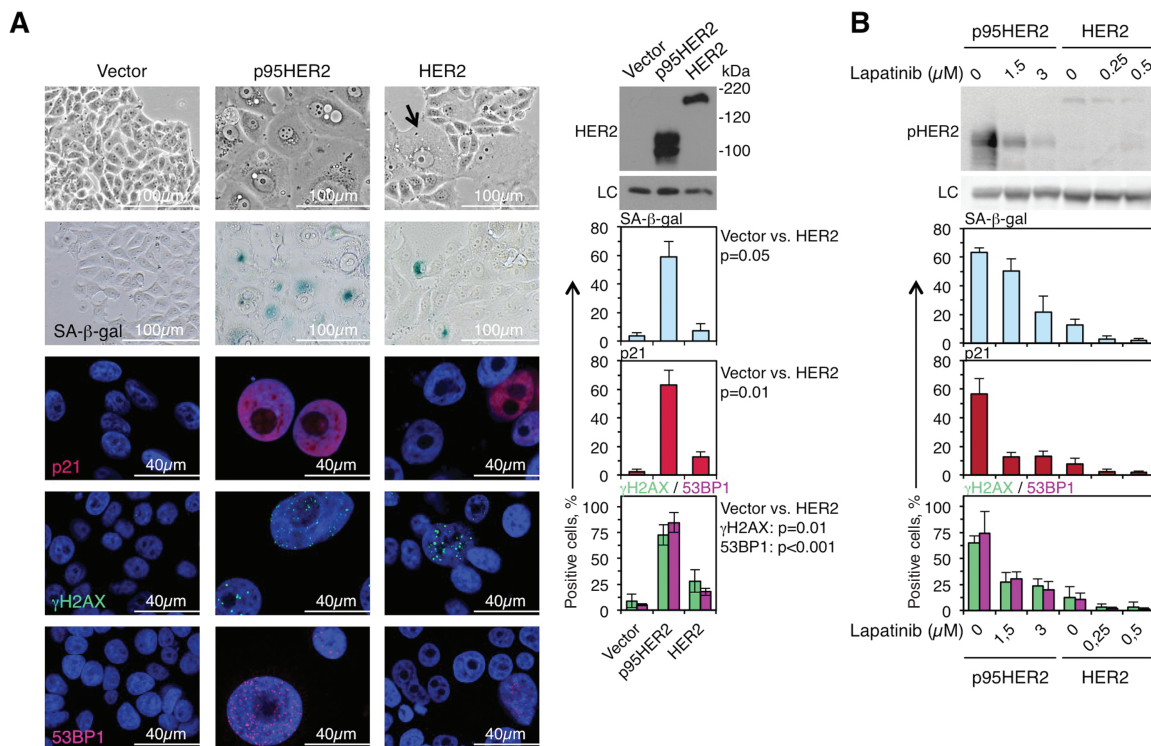


**Figure 1.** The percentage of senescent cells is directly proportional to the intensity of HER2 signaling. **A)** MCF7 Tet-Off cells stably transfected with an empty vector or with the same vector expressing p95HER2 or HER2 under the control of a doxycycline-responsive element were cultured for seven days in the absence of doxycycline. Then, cells were photographed under bright field, analyzed by western blot with antibodies against HER2, stained for SA-β-gal or immunostained for p21, gammaH2AX, or 53BP1. DAPI was used to visualize nuclei; representative bright field and confocal immunofluorescence images are shown. As indicated, the percentages of positive cells were quantified in four independent analyses and expressed as averages. **B)** The same cells as in **A** were cultured without doxycycline and treated with different concentrations of lapatinib. After one week, cells were analyzed by western blot with antibodies against phosphoHER2, and cells positive for the indicated markers were quantified as in **(A)**. The results are expressed as averages. Error bars correspond to 95% confidence intervals.

5.938%],  $P < .001$ ; gammaH2AX: 28.0% [95% CI = 13.84% to 42.27%] vs 8.8% [95% CI = 0.844% to 16.90%],  $P = .01$ ; and 53BP1: 17.6% [95% CI = 13.43% to 22.80%] vs 5.1% [95% CI = 3.443% to 6.757%],  $P < .001$  (Figure 1A). Confirming that the percentage of senescent cells was directly proportional to the intensity of HER2 signaling, treatment with different concentrations of lapatinib, a tyrosine kinase inhibitor that targets HER2, lowered the percentages of cells expressing the markers of senescence in a dose-dependent manner (MCF7/p95HER2 treated with DMSO, 1.5  $\mu$ M lapatinib or 3  $\mu$ M lapatinib, respectively: SA- $\beta$ -Gal: 63.4%, 50.5%, and 21.7%; p21: 56.5%, 12.9%, and 13.1%, gammaH2AX: 64.7%, 27.4%, and 23.5%; and 53BP1: 74.2%, 30.2%, and 19.9%; MCF7/HER2 treated with DMSO, 0.25  $\mu$ M lapatinib or 0.5  $\mu$ M lapatinib, respectively: SA- $\beta$ -Gal: 11.1%, 1.7%, and 0.7%; p21: 7.6%, 2.4%, and 1.8%; gammaH2AX: 12.6%, 3.5%, and 3.2%; and 53BP1: 10.6%, 1.7%, and 1.6%) (Figure 1B). Since MCF7 cells do not depend on HER2 signaling, lapatinib did not affect the proliferation of the same cells transfected with full-length HER2. In contrast and consistent with its ability to interfere with the onset of HER2-driven senescence, lapatinib increased the proliferation and percentage in S-phase of cells expressing p95HER2 (cell number relative to day 0: 9.15 [95% CI = 0.82 to 17.47] [3  $\mu$ M lapatinib] vs 0.89 [95% CI = 0.76 to 1.02] [DMSO],  $P = .006$ ) (Supplementary Figure 1C, available online).

Cells with the morphology of senescent cells and positive for SA- $\beta$ -gal were observed in cultures of HCC1954, SkBr3, and BT474 cells (Figure 2A). In cultures of MDA-MB-453 cells, we observed enlarged cells that, despite not having the characteristic flattened morphology of senescent cells, were positive for SA- $\beta$ -gal (Figure 2A). The rest of the senescence markers were also detected in 2% to 5% of the cells (SA- $\beta$ -Gal, p21, gammaH2AX, and 53BP1 values: HCC1954: 4.5%, 4.9%, 4.2%, and 3.9%; SkBr3: 3.4%, 5.7%, 10.4%, and 8.4%; BT474: 2.3%, 2.7%, 3.1%, and 0.7%; and MDA-MB-453: 2.6%, 4.8%, 9.1%, and 3.9%) (Figure 2A). Costaining with anti-p21 and anti-gammaH2AX showed an association between these markers that was statistically significant in all cell lines (percentage of gammaH2AX: HCC1954, 41.6% of p21(+) vs 2.7% of p21(-),  $P < .001$ ; BT474: 31.5% of p21(+) vs 10.3% of p21(-),  $P = .01$ ; SkBr3, 35.7% of p21(+) vs 5.4% of p21(-),  $P = .001$ ; and MDA-MB-453, 53.8% of p21(+) vs 7.2% of p21(-),  $P < .001$ ) (Figure 2B). Thus, these markers tend to be expressed in the same cells. In summary, senescent cells arise during the culture of cell lines naturally overexpressing HER2.

The kinetics of decay of carboxyfluorescein succinimidyl ester (CFSE) from control MCF7 cells or the same cells expressing p95HER2 or HER2 confirmed the feasibility of using the fluorescent dye to isolate senescent cells; fluorescence was lost much more rapidly in the proliferating cell cultures than in p95HER2-induced senescent cells (Supplementary Figure 2A, available online). Further, consistent with the higher percentage of senescent cells in cultures from MCF7/HER2 cells than in cultures from MCF7/Vector cells (Figure 1A), the percentage of label-retaining MCF7/HER2 cells (MCF7/HER2<sup>CFSE hi</sup>) was statistically significantly higher than that of MCF7/Vector cells (MCF7/Vector<sup>CFSE hi</sup>) (MCF7/Vector:  $0.90 \pm 0.2$  vs MCF7/HER2:  $1.60 \pm 0.75$ ,  $P = .04$ ) (Supplementary Figure 2B, available online). Quantification of SA- $\beta$ -gal and nuclear p21 expression in the MCF7/HER2<sup>CFSE hi</sup> and MCF7/HER2<sup>CFSE lo</sup> subpopulations, sorted from cells labeled and cultured for two weeks, showed approximately a four-fold enrichment in the percentage of senescent cells in the former (MCF7/HER2 CFSE Hi vs CFSE Lo cells; SA- $\beta$ -Gal: 25.4% [95% CI = 18.66% to 32.28%] vs 5.4% [95% CI = 3.14% to 7.76%],  $P < .001$ ; and p21 23.1% [95% CI = 12.77% to 33.54%] vs 7.1% [95% CI = 2.27% to 10.98%],  $P = .002$ ) (Supplementary Figure 2C, available online). Similar results were obtained with PKH26 as labeling reagent (data not shown). Using the same procedure, we isolated HCC1954<sup>CFSE hi</sup> cells (Figure 3A). In this fraction we also observed approximately a four-fold increase in the percentage of senescent cells relative to that in the HCC1954<sup>CFSE lo</sup> fraction (percentage of positive cells in CFSE hi vs CFSE lo: SA- $\beta$ -Gal, 25.0% [95% CI = 19.45% to 30.58%] vs 8.0% [95% CI = 2.63% to 13.50%],  $P < .001$ ; p21, 17.6% [95% CI = 10.69% to 24.59%] vs 4.9% [95% CI = 2.93% to 7.06%],  $P = .001$ ; and gammaH2AX, 20.3% [95% CI = 11.79% to 28.77%] vs 4.3% [95% CI = 2.03% to 6.64%],  $P = .001$ ; 53BP1, n.s.) (Figure 3B).

To determine if naturally occurring senescent HCC1954 cells exhibit a secretory phenotype, we firstly measured the levels of different factors (IL-6, IL-8, and AREG) previously shown to be secreted by p95HER2-induced senescent cells (6). The levels of these factors were statistically significantly higher in the media conditioned by HCC1954<sup>CFSE hi</sup> cells with respect to HCC1954<sup>CFSE lo</sup> (IL-6: 5.06 pg/mL [95% CI = -1.16 pg/mL to 11.28 pg/mL] vs 0.82 pg/mL [95% CI = -0.04 pg/mL to 1.68 pg/mL],  $P = .01$ ; IL-8: 202.51 pg/mL [95% CI = 105.2 pg/mL to 299.7 pg/mL] vs 55.21 pg/mL [95% CI = 4.29 pg/mL to 106.2 pg/mL],  $P = .005$ ; and AREG: 233.28 pg/mL [95% CI = 21.47 pg/mL to 445.1 pg/mL] vs 48.28 pg/mL [95% CI = 26.87 pg/mL

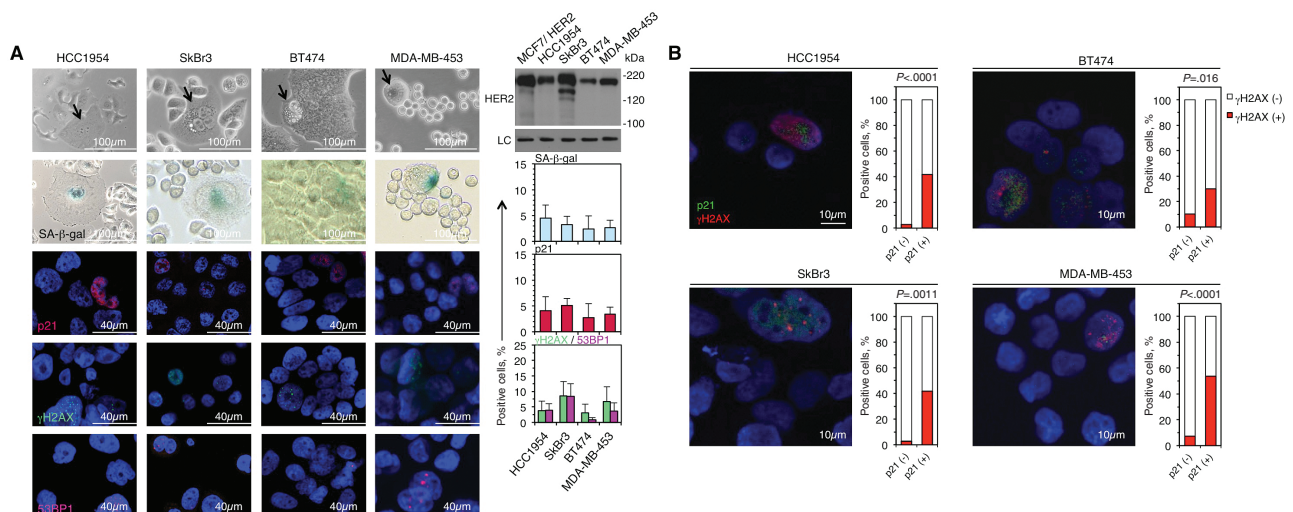


**Figure 2.** Identification of naturally occurring senescent cells in cultures of HER2-positive cell lines. **A)** The indicated cell lines were analyzed as described in the legend to Figure 1A. **B)** Cells were coimmunostained with antibodies against p21 and gammaH2AX; representative confocal immunofluorescence images of cells expressing both markers are shown. Positive cells for p21 and/or gammaH2AX were counted and represented as percentages.

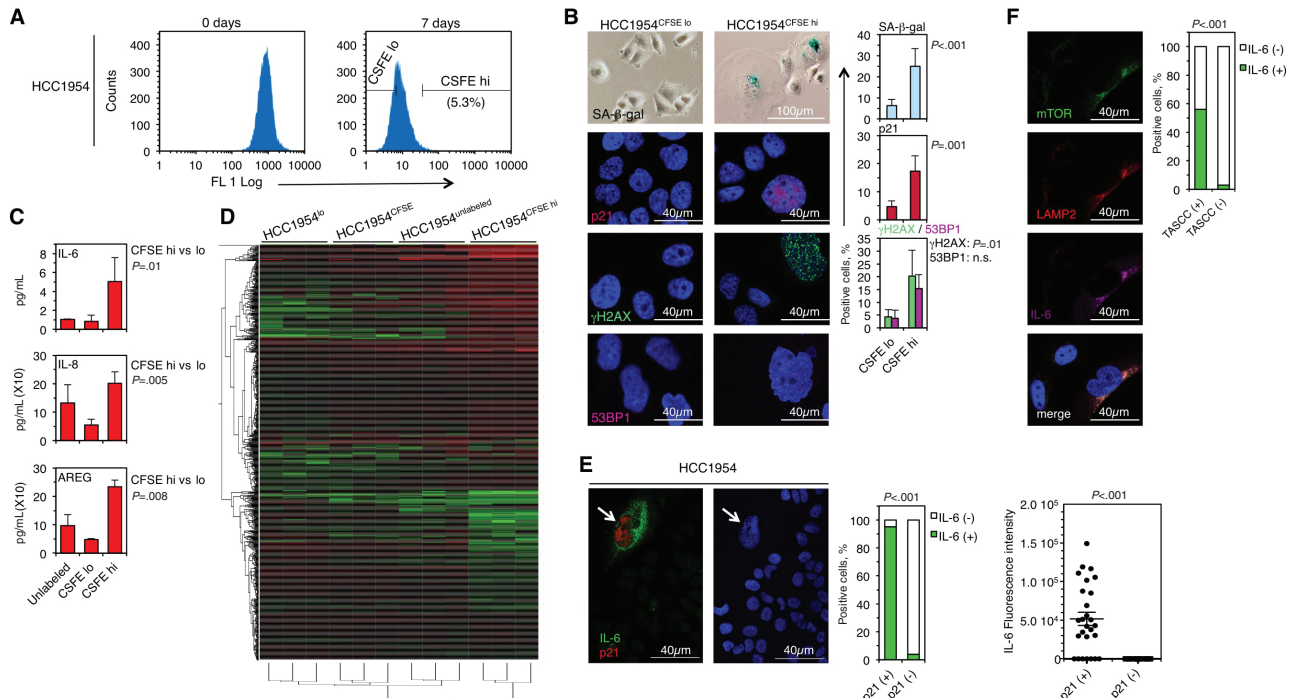


**Figure 3.** Secretory phenotype of naturally occurring HCC1954-senescent cells. **A)** HCC1954 cells were labeled with CFSE and analyzed by flow cytometry right after labeling or cultured for seven days before analysis. At this time,  $^{CFSE\ lo}$  and  $^{CFSE\ hi}$  cells were gated as shown for subsequent purification by cell sorting. **B)** HCC1954 $^{CFSE\ lo}$  and  $^{CFSE\ hi}$  cells were stained for the indicated markers; representative bright field and confocal images are shown. The percentages of positive cells were quantified in three independent experiments and expressed as averages. **Error bars** correspond to 95% confidence intervals. **C)** The levels of the indicated factors in the media conditioned by control HCC1954, HCC1954 $^{CFSE\ lo}$  or HCC1954 $^{CFSE\ hi}$  cells were analyzed by enzyme-linked immunosorbent assay. The results are averages of three independent experiments. **D)** The secretomes of HCC1954 $^{CFSE\ lo}$  or HCC1954 $^{CFSE\ hi}$  or, as controls, those of unlabeled or labeled ( $^{-CFSE}$ ) HCC1954 cells were analyzed by label-free quantitative proteomics. The results are shown as unsupervised hierarchical clustering analysis of three replicates. **E)** HCC1954 cells were coimmunostained with antibodies against IL-6 and p21; representative confocal immunofluorescence images are shown. The **arrow** marks a cell positive for p21 and IL-6 (left) and its corresponding nucleus stained with DAPI (right). Positive cells for IL-6 and/or p21 were counted and represented as percentages. IL-6 fluorescence intensity was determined for each cell and plotted in two groups, according to nuclear p21 staining. **F)** HCC1954 cells were coimmunostained with antibodies against mTOR, LAMP2, and IL-6. Nuclei were stained with DAPI. A confocal immunofluorescence image representative of one TASSC- and IL-6-positive cell is shown. Positive cells for IL-6 and/or TASSC were counted and represented as percentages. **Error bars** correspond to 95% confidence intervals.

to 69.68 pg/mL,  $P = .008$  (Figure 3C). Furthermore, analysis of the media conditioned by control HCC1954, HCC1954 $^{CFSE\ lo}$ , and HCC1954 $^{CFSE\ hi}$  cells through quantitative label-free proteomics confirmed that the latter have a distinct secretory phenotype (Figure 3D; Supplementary Table 1, available online).

Although senescent cells accumulate in the HCC1954 $^{CFSE\ hi}$  fraction, this subpopulation may also contain slow proliferating cells and/or other cells that retain the fluorescent dye for unknown reasons. To characterize the cells that produce the factors analyzed in Figure 3C, we costained cells with antibodies against p21 as a marker of senescence and antibodies against the component of the senescence secretome IL-6. We found that the majority (95.1%) of p21-positive cells expressed IL-6, while less than 5% of p21-negative cells expressed detectable levels of the cytokine ( $P < .001$ ) (Figure 3E). Furthermore, the median intensity of fluorescence corresponding to IL-6 in p21-positive cells was much higher than that in the few p21-negative cells that expressed detectable levels of IL-6 (IL-6 intensity: 54546 AU in p21(+) [95% CI = 36150 AU to 72942 AU] vs 0.0 AU in p21(-) cells [95% CI = 0.0 AU to 0.0 AU],  $P < .001$ ) (Figure 3E). Similar results were obtained with IL-8, albeit the number of p21-positive cells that had high levels of IL-8 expression was lower (~20%) (percentage of IL-8(+) cells: 19.4% in p21(+) vs 1.1% in p21(-) cells,  $P < .001$ ) (Supplementary Figure 3A, available online).

Compared with the corresponding  $^{CFSE\ lo}$  cells, SkBr3 $^{CFSE\ hi}$ , and MDA-MB-453 $^{CFSE\ hi}$  cells also secreted higher levels of IL-6 (SkBr3: 0.08 pg/mL in CFSE Hi [95% CI = -0.02 pg/mL to 0.18 pg/mL] vs

0.01 pg/mL in CFSE Lo [95% CI = -0.01 pg/mL to 0.03 pg/mL],  $P = .02$ ; MDA-MB-453: 0.06 pg/mL in CFSE Hi [95% CI = 0.0 pg/mL to 0.12 pg/mL] vs 0.01 pg/mL in CFSE Lo [95% CI = -0.01 pg/mL to 0.03 pg/mL],  $P = .03$ ) (Supplementary Figure 3B, available online). We could not, however, detect IL-6 by immunofluorescence in these cell lines. This was likely because they produced levels of the cytokine below the threshold of detection.

We concluded that the secretion of IL-6 and other cytokines by the HER2-positive cell lines analyzed are mainly, if not exclusively, carried out by naturally occurring senescent cells.

To further characterize the secretory phenotype of naturally occurring senescent cells, we studied the presence of TASSC. We observed discrete regions of colocalization of mTOR with the lysosomal marker LAMP2, a hallmark of the TASSC, in approximately 7% of HCC1954 cells. The percentage of TASSC-positive cells was increased in the HCC1954 $^{CFSE\ hi}$  fraction (percentage of TASSC(+) cells: 15.5% in CFSE hi [95% CI = 11.02% to 20.01%] vs 3.4% in CFSE lo [95% CI = 0.48% to 6.50%],  $P < .001$ ) (Supplementary Figure 3C, available online), indicating that this subcellular compartment could be responsible for the production of IL-6 in naturally occurring senescent cells. Supporting this possibility, IL-6 was expressed in approximately 60% of TASSC-positive cells (Figure 3F).

To verify that senescent cells are also present in tumors in vivo and are not cleared by the immune system, we analyzed SA-β-gal in fresh samples from HER2-driven mammary tumors developed in transgenic mice. In line with published reports (25), 5% to 10% of the cells expressed the senescence

marker in advanced tumors (Supplementary Figure 4A, available online). Because of technical limitations, cells producing IL-6 could not be stained with specific antibodies in fixed tumor samples; thus, to determine if senescent cells produced IL-6, we stained tumor cells obtained from transgenic mice with PKH26. After six days in culture, IL-6 was detected almost exclusively in cells retaining PKH26 (percentage of IL-6(+) cells: 29.5% in PKH26(+) vs 0.3% in PKH26(-) cells,  $P < .001$ ) (Supplementary Figure 4B, available online). As expected, approximately 50% of PKH26-positive cells were also positive for SA- $\beta$ -gal (Supplementary Figure 4C, available online), indicating that senescent cells are those predominantly expressing IL-6 also in these HER2-driven tumors.

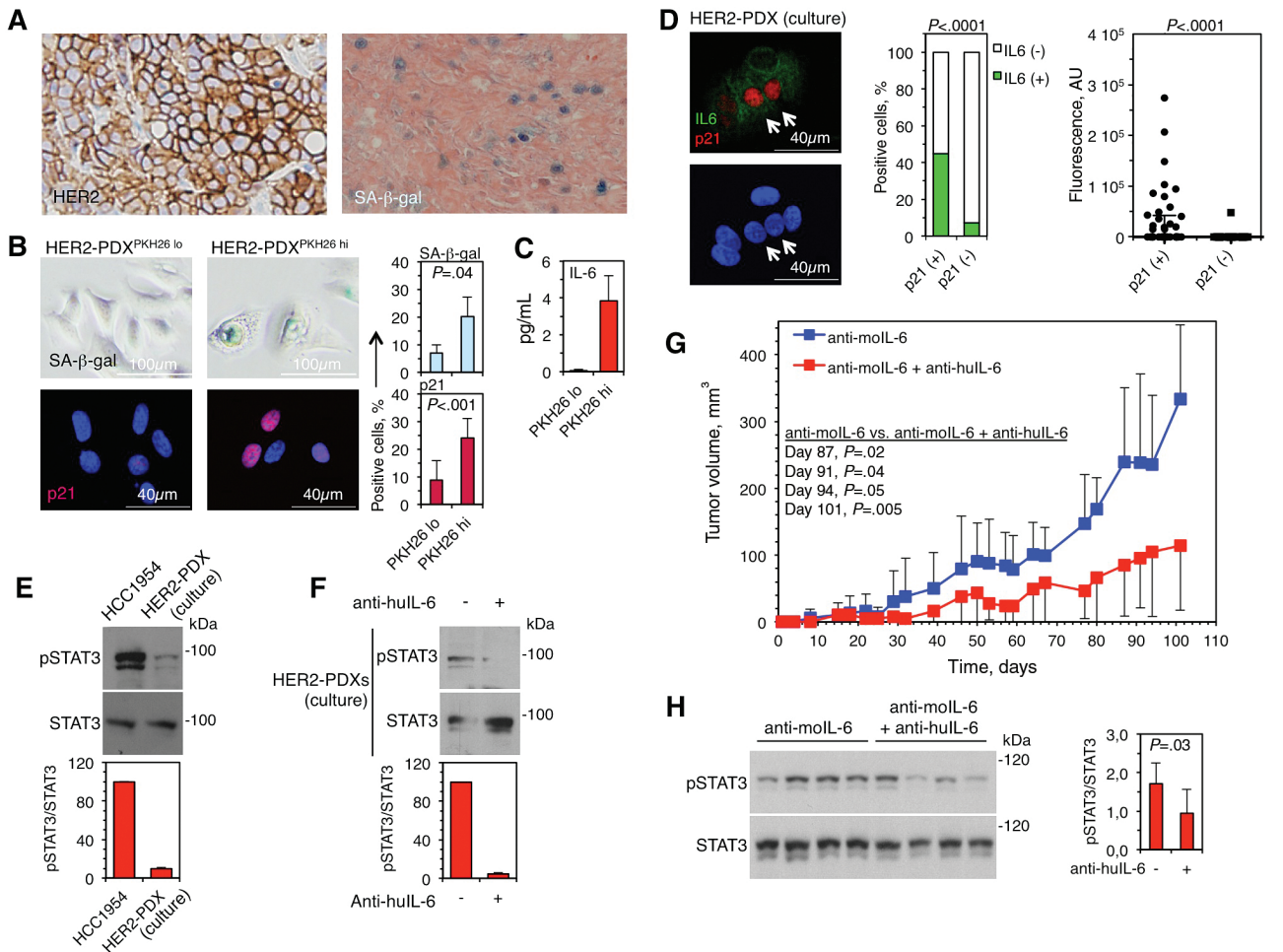


**Figure 4.** Naturally occurring senescent cells from a HER2-expressing patient-derived xenograft secrete IL-6, which is required for tumor growth. **A)** A HER2-positive PDX orthotopically implanted into NOD/SCID mice was allowed to grow to approximately 300 mm<sup>3</sup>. Then, the tumor was surgically removed and samples from it were immunostained with antibodies against HER2 or stained for SA- $\beta$ -gal. **B)** PKH26<sup>lo</sup> and PKH26<sup>hi</sup> cells sorted from HER2-PDX cell cultures as described in Figure S2 (available online) and Figure 3A were stained with the indicated markers to quantify the presence of senescent cells. Representative confocal images are shown. The percentages of positive cells were quantified in three independent experiments and expressed as averages. **C)** The levels of IL-6 in the media conditioned by PKH26<sup>lo</sup> and PKH26<sup>hi</sup> cells from the HER2-PDX were determined by enzyme-linked immunosorbent assay. Quantitative results are averages of duplicate determinations. **D)** Cultures from the HER2-PDX cells were coimmunostained with antibodies against IL-6 and p21; representative confocal immunofluorescence images are shown. The arrows mark cells positive for p21 and IL-6 (top) and the corresponding nucleus stained with DAPI (bottom). Positive cells for IL-6 and/or p21 were counted and represented as percentages. IL-6 fluorescence intensity was determined for each cell and plotted in two groups, according to nuclear p21 staining. **E)** Cultures from HCC1954 cells and from the HER2-PDX were starved from serum for 48 hours. Then, cells were lysed and the cell lysates were analyzed by Western blot with specific antibodies against phospho-STAT3 or STAT3. Quantitative results are averages of two independent experiments. **F)** Cultures from the HER2-PDX were serum-starved and treated with or without anti-huIL-6 (10 ng/mL) for 48 hours. Then, cells were lysed and the cell lysates were analyzed by western blot with specific antibodies against phospho-STAT3 or STAT3. Quantitative results are averages of two independent experiments. **G)** The HER2-PDX was orthotopically implanted into NOD/SCID mice ( $n = 6$  in each group). Tumor volumes were determined at the indicated time points and expressed as averages. As indicated, mice were treated with antimouse IL-6 or antimouse IL-6 and antihuman IL-6 (siltuximab). **H)** At the end of the experiment described in Figure 4G, tumors were surgically removed and lysed. Cell lysates corresponding to four independent tumors from each group were analyzed by western blot with specific antibodies against phospho-STAT3 or STAT3. Results were quantified and represented as averages. Error bars correspond to 95% confidence intervals.

Because the activation of the JAK-STAT pathway by IL-6 is required for the growth of HER2-driven tumors (16) and virtually all the IL-6 produced by HCC1954 cultures is secreted by senescent cells (Figure 3E), this cell line is, in principle, a suitable model to show the importance of cellular senescence during tumor growth in vivo. Thus, we injected HCC1954 cells into the mammary fat pad of Balb/C nude mice. To block alternative sources of IL-6, which can be produced by a variety of stromal cells including monocytes, fibroblasts, and endothelial cells (28), we treated the mice with an antimouse IL-6 (moIL-6) that does not recognize human IL-6 (huIL-6). Under these conditions, treatment with anti-huIL-6, had little effect on tumor growth (Supplementary Figure 5A, available online).

This result argues that either activation of the JAK-STAT pathway is not required for the growth of HCC1954 cells in vivo or that other cytokines activate the pathway in these cells. In support of the latter, the levels of activation of the JAK-STAT pathway in serum-starved cells, as measured by the levels of phospho-STAT3 (Supplementary Figure 5B, available online), is not affected by anti-huIL-6 blocking antibodies. We concluded that, in contrast to other HER2-driven tumor models, which depend on IL-6 to progress (16), HCC1954 cells have alternative ways to activate the JAK-STAT pathway. Therefore, we used another model to test the relevance of IL-6-producing senescent cells during tumor growth.

Patient-derived xenografts (PDXs) retain many of the characteristics of the original tumor from which they are derived. Approximately five percent of the cells of a PDX established from a HER2-positive breast cancer (see [29]) were positive for SA- $\beta$ -gal (Figure 4A), showing that also in this model senescent cells are continuously generated during tumor growth. To characterize these senescent cells, we established cultures from the HER2-PDX and sorted PKH26-retaining cells. Confirming the results shown in Figure 3, the HER2-PDX<sup>PKH26<sup>hi</sup></sup> subpopulation was enriched in senescent cells (percentage of SA- $\beta$ -Gal(+) cells: 18.0% in PKH26<sup>hi</sup> [95% CI = 6.94% to 29.23%] vs 7.0% in PKH26<sup>lo</sup> [95% CI = -0.33% to 14.39%],  $P = .04$ ; percentage of p21(+) cells: 23.9% in PKH26<sup>hi</sup> [95% CI = 13.74% to 34.22%] vs 7.7% in PKH26<sup>lo</sup> [95% CI = 4.49% to 11.05%],  $P < .001$ ) (Figure 4B), secreted higher levels of IL-6 (Figure 4C), and the cytokine was largely produced by p21-positive cells (percentage of IL-6(+) cells: 45.0% of p21(+) vs 7.1% of p21(-) cells,  $P < .001$ ) (Figure 4D). We concluded that the senescent cells from the HER2-positive PDX are also responsible for the secretion of IL-6.

The basal level of activation of the JAK-STAT pathway is lower in cultures of the HER2-PDX than in HCC1954 cells (Figure 4E). Since both cell types secrete similar levels of IL-6 (Figures 3C and 4C), this result further supports that additional cytokines activate the JAK-STAT pathway in HCC1954 cells. Treatment with anti-huIL-6 lowered the levels of phospho-STAT3 in the HER2-PDX cells (Figure 4F), showing that in these cultures the IL-6 produced by senescent cells activates the JAK-STAT pathway in an autocrine/paracrine fashion. Importantly, treatment of mice bearing the HER2-PDX with anti-huIL-6 showed that IL-6, which is produced largely by senescent cells, is required for tumor growth (tumor volume at day 101: 333.2mm<sup>3</sup> [control] [95% confidence interval = 216.6 mm<sup>3</sup> to 449.8 mm<sup>3</sup>] vs 114.4 mm<sup>3</sup> [anti-huIL-6 treated] [95% CI = 12.79 mm<sup>3</sup> to 216.0 mm<sup>3</sup>],  $P = .005$ ) (Figure 4G). Analysis of phospho-STAT3 levels confirmed that blocking of human IL-6 resulted in the inhibition of the JAK-STAT pathway in vivo (Figure 4H).

## Discussion

To date, more than 50 oncogenes have been found to induce senescence (30). Previous reports showed that, in order to trigger OIS, the signals conveyed by these oncogenes should reach a certain threshold of intensity. For example, using an in vivo-inducible system, it has been shown that high levels of activated Ras induce OIS very efficiently, but below certain threshold of expression Ras promotes cellular proliferation (31). Similarly, according to our results, HER2-induced senescence does not respond to an all-or-none model. We observed that different levels of HER2 signaling result in different percentages of cells undergoing senescence.

In breast and other tumors, HER2 is activated through gene amplification, but analysis of individual tumors shows that HER2 gene copy number is extremely variable. As a result, the levels of HER2 protein expression in different tumors show a wide dynamic range that extends well over two orders of magnitude

(17,18). Conceivably, in some amplified tumors the levels of HER2 could be precisely those that lead to the onset of senescence in only a percentage of cells.

The activity of other oncogenes activated through mutation, such as RAS or BRAF, probably do not have such a dynamic range and thus may preferentially induce senescence in the majority, if not all, of the cells that express them. Consistently with this view, oncogene-induced senescence is readily detected in premalignant lesions induced by K-RasV12 in lungs and pancreas, but is not detected in adenocarcinomas (reviewed in [32]), once OIS has been overcome. In contrast, in mammary tumors driven by HER2 or prostate tumors genetically deficient for PTEN, the generation of senescent cells remain constant during tumor progression representing, by some estimates, 20% to 30% of the total tumor cellularity (25,33).

The fact that naturally arising senescent cells display a senescence secretome that includes IL-6 is relevant to the progression of breast cancers. In fact, in the models analyzed here, only senescent cells produce high levels of IL-6. Since this cytokine is required for the progression of HER2-driven tumors in vivo, these results demonstrate that senescence, a potent antitumor mechanism, can be perverted in order to generate factors that foster the growth of nonsenescent cells.

This study also had some limitations. Currently there are no markers of senescence for use in clinically relevant samples, making it difficult to extrapolate our results to the clinical setting. In addition, in some of the models analyzed we have detected senescent cells by the expression of p21, which may be also expressed in nonsenescent cells. The identification of novel marker of senescence, particularly if they can be used in clinically relevant samples, will allow overcoming these shortcomings.

## Funding

Supported by funds from The Breast Cancer Research Foundation (BCRF), Spanish Association Against Cancer (Asociación Española Contra el Cáncer, AECC), AVON Cosmetics, Instituto de Salud Carlos III (Research Project PI12/02536, selected within the frame of an operative program co-funded by ERDF (European Regional Development Fund)) and “Red Temática de investigación cooperativa en cáncer” (translated as Network of Cooperative Cancer Research) (RTICC-RD12/0036/0042) to JA and (PI11/02496) to IR.

## Notes

The study funders had no role in the design of the study, the collection, analysis, or interpretation of the data, the writing of the manuscript, nor the decision to submit the manuscript for publication.

We are grateful to Dr. Yi Li, Irene Sales Pardo, and Marta Valeri Sala from the Unidad de Alta Tecnología, Vall d’Hebron Institut de Recerca (High Technology Unit, Vall d’Hebron Research Institute) for technical support and members of the Arribas and Serra laboratories for helpful discussions.

## References

- Collado M, Gil J, Efeyan A, et al. Tumour biology: senescence in premalignant tumours. *Nature*. 2005;436(7051):642-642.
- Coppé J-PJ, Patil KKC, Rodier FF, et al. Senescence-associated secretory phenotypes reveal cell-nonautonomous functions of oncogenic RAS and the p53 tumor suppressor. *PLoS Biol*. 2008;6(12):2853-2868.
- Kuilman T, Peeper DS. Senescence-messaging secretome: SMS-ing cellular stress. *Nat Rev Cancer*. 2009;9(2):81-94.
- Narita M, Young ARJ, Arakawa S, et al. Spatial coupling of mTOR and autophagy augments secretory phenotypes. *Science*. 2011;332(6032):966-970.

5. Chanarat S, Seizl M, Strasser K. Senescent cells develop a PARP-1 and nuclear factor- $\kappa$ B-associated secretome (PNAS). *Genes Dev.* 2011;25(12):1245–1261.
6. Angelini PD, Zacarias Fluck MF, Pedersen K, et al. Constitutive HER2 signaling promotes breast cancer metastasis through cellular senescence. *Cancer Res.* 2013;73(1):450–458.
7. Acosta JC, O'Loughlin A, Banito A, et al. Chemokine Signaling via the CXCR2 Receptor Reinforces Senescence. *Cell.* 2008;133(6):1006–1018.
8. Kuilman T, Michaloglou C, Vredeveld LCW, et al. Oncogene-Induced Senescence Relayed by an Interleukin-Dependent Inflammatory Network. *Cell.* 2008;133(6):1019–1031.
9. Lujambio A, Akkari L, Simon J, et al. Non-cell-autonomous tumor suppression by p53. *Cell.* 2013;153(2):449–460.
10. Kang T-W, Yevsa T, Woller N, et al. Senescence surveillance of pre-malignant hepatocytes limits liver cancer development. *Nature.* 2012;479(7374):547–551.
11. Ventura A, Kirsch DG, McLaughlin ME, et al. Restoration of p53 function leads to tumour regression in vivo. *Nature.* 2007;445(7128):661–665.
12. Xue W, Zender L, Miething C, et al. Senescence and tumour clearance is triggered by p53 restoration in murine liver carcinomas. *Nature.* 2007;445(7128):656–660.
13. Gradishar WJ. HER2 therapy—an abundance of riches. *N Engl J Med.* 2012;366(2):176–178.
14. Ginestier C, Liu S, Diebel ME, et al. CXCR1 blockade selectively targets human breast cancer stem cells in vitro and in xenografts. *J Clin Invest.* 2010;120(2):485–497.
15. Korkaya H, Kim G-I, Davis A, et al. Activation of an IL6 inflammatory loop mediates trastuzumab resistance in HER2+ breast cancer by expanding the cancer stem cell population. *Mol Cell.* 2012;47(4):570–584.
16. Hartman ZC, Yang X-Y, Glass O, et al. HER2 overexpression elicits a proinflammatory IL-6 autocrine signaling loop that is critical for tumorigenesis. *Cancer Res.* 2011;71(13):4380–4391.
17. Huang W, Reinholz M, Weidler J, et al. Comparison of Central HER2 Testing With Quantitative Total HER2 Expression and HER2 Homodimer Measurements Using a Novel Proximity-Based Assay. *Am J Clin Pathol.* 2010;134(2):303–311.
18. Sperinde J, Jin X, Banerjee J, et al. Quantitation of p95HER2 in paraffin sections by using a p95-specific antibody and correlation with outcome in a cohort of trastuzumab-treated breast cancer patients. *Clin Cancer Res.* 2010;16(16):4226–4235.
19. Parra-Palau JL, Pedersen K, Peg V, et al. A major role of p95/611-CTF, a carboxy-terminal fragment of HER2, in the down-modulation of the estrogen receptor in HER2-positive breast cancers. *Cancer Res.* 2010;70(21):8537–8546.
20. Pedersen K, Angelini PD, Laos S, et al. A naturally occurring HER2 carboxy-terminal fragment promotes mammary tumor growth and metastasis. *Mol Cell Biol.* 2009;29(12):3319–3331.
21. Trost TM, Lausch EU, Fees SA, et al. Premature senescence is a primary fail-safe mechanism of ERBB2-driven tumorigenesis in breast carcinoma cells. *Cancer Res.* 2005;65(3):840–849.
22. Burgess A, Vigneron S, Brioudes E, et al. Loss of human Greatwall results in G2 arrest and multiple mitotic defects because of deregulation of the cyclin B-Cdc2/PP2A balance. *Proc Natl Acad Sci U S A.* 2010;107(28):12564–12569.
23. Parra-Palau JL, Morancho B, Peg V, et al. Effect of p95HER2/611CTF on the Response to Trastuzumab and Chemotherapy. *J Natl Cancer Inst.* 2014;106(11): In press.
24. Campeau E, Ruhl VE, Rodier F, et al. A Versatile Viral System for Expression and Depletion of Proteins in Mammalian Cells. *PLoS ONE.* 2009;4(8):e6529.
25. Reddy JP, Peddibhotla S, Bu W, et al. Defining the ATM-mediated barrier to tumorigenesis in somatic mammary cells following ErbB2 activation. *Proc Natl Acad Sci U S A.* 2010;107(8):3728–3733.
26. Du ZZ, Podsypanina KK, Huang SS, et al. Introduction of oncogenes into mammary glands in vivo with an avian retroviral vector initiates and promotes carcinogenesis in mouse models. *Proc Natl Acad Sci U S A.* 2006;103(46):17396–17401.
27. d'Adda di Fagagna F. Living on a break: cellular senescence as a DNA-damage response. *Nat Rev Cancer.* 2008;8(7):512–522.
28. Chang Q, Daly L, Bromberg J. Seminars in Immunology. *Semin Immunol.* 2014;26(1):48–53.
29. Morancho B, Parra-Palau JL, Ibrahim YH, et al. A dominant-negative N-terminal fragment of HER2 frequently expressed in breast cancers. *Oncogene.* 2013;32(11):1452–1459.
30. Gorgoulis VG, Halazonetis TD. Oncogene-induced senescence: the bright and dark side of the response. *Curr Opin Cell Biol.* 2010;22(6):12–12.
31. Sarkisian CJ, Keister BA, Stairs DB, Boxer RB, Moody SE, Chodosh LA. Dose-dependent oncogene-induced senescence in vivo and its evasion during mammary tumorigenesis. *Nat Cell Biol.* 2007;9(5):493–505.
32. Collado M, Serrano M. Senescence in tumours: evidence from mice and humans. *Nat Rev Cancer.* 2010:51–57.
33. Toso A, Revandkar A, Di Mitri D, et al. Enhancing Chemotherapy Efficacy in Pten-Deficient Prostate Tumors by Activating the Senescence-Associated Antitumor Immunity. *Cell Rep.* 2014;9(1):75–89.
34. Krishan A. Rapid flow cytofluorometric analysis of mammalian cell cycle by propidium iodide staining. *J Cell Biol.* 1975;66(1):188–193.